Original Paper

Cellular Physiology and Biochemistry

Cell Physiol Biochem 2012;29:583-594

Accepted: January 05, 2012

Ganoderma Lucidum Polysaccharide Accelerates Refractory Wound Healing by Inhibition of Mitochondrial Oxidative Stress in Type 1 Diabetes

Lu Tie[1], Hong-Qin Yang[1,3], Yu An[1], Shao-Qiang Liu[1,4], Jing Han[1], Yan Xu[1], Min Hu[1], Wei-Dong Li[1], Alex F. Chen[2], Zhi-Bin Lin[1] and Xue-Jun Li[1]

[1]State Key Laboratory of Natural & Biomimetic Drugs, Department of Pharmacology, School of Basic Medical Sciences, and Institute of System Biomedicine, Peking University, Beijing, [2]Department of Surgery, Vascular Medicine Institute and McGowan Institute of Regenerative Medicine, University of Pittsburgh School of Medicine, Pittsburgh, PA, [3]Baoshan Chinese Traditional Medical College, Baoshan, [4]Peking University Third Hospital, Beijing

Key Words

Ganoderma lucidum polysaccharide (*Gl*-PS) • Oxidative stress • Mitochondria • Diabetes • Manganese superoxide dismutase (MnSOD) • p66Shc • Nitrotyrosine

Abstract

Background/Aims. Refractory wounds in diabetic patients constitute a serious complication that often leads to amputation with limited treatment regimens. The present study was designed to determine the protective effect of *Ganoderma lucidum* polysaccharide (*Gl*-PS) on diabetic wound healing and investigate underlying mechanisms. Methods. Streptozotocin (STZ)-induced type 1 diabetic mice with full-thickness excisional wounds were intragastrically administered with 10, 50 or 250 mg/kg/day of *Gl*-PS. Results. *Gl*-PS dose-dependently rescued the delay of wound closure in diabetic mice. 50 and 250 mg/kg/day of *Gl*-PS treatment significantly increased the mean perfusion rate around the wound in diabetic mice. Diabetic conditions markly increased mitochondrial superoxide anion ($O_2^{\cdot -}$) production, nitrotyrosine formation, and inducible nitric oxide synthase (iNOS) activity in wound tissues, which were normalized with *Gl*-PS treatment. In diabetic wound tissues, the protein level of manganese superoxide dismutase (MnSOD) was unchanged whereas MnSOD activity was inhibited and its nitration was potentiated; *Gl*-PS administration suppressed MnSOD nitration and increased MnSOD and glutathione peroxidase (GPx) activities. Moreover, *Gl*-PS attenuated the redox enzyme p66Shc expression and phosphorylation dose-dependently in diabetic mice skin. Conclusion. *Gl*-PS rescued the delayed wound healing and improved wound angiogenesis in STZ-induced type 1 diabetic mice, at least in part, by suppression of cutaneous MnSOD nitration, p66Shc and mitochondrial oxidative stress.

Introduction

Impaired cutaneous wound healing in diabetic patients is a serious complication that often leads to amputation [1]. It is estimated that every 30 seconds a lower limb is lost worldwide as a result of diabetes with limited treatment regimens [2]. Various factors contribute to impaired diabetic wound healing, including inflammatory

KARGER

Fax +41 61 306 12 34
E-Mail karger@karger.ch
www.karger.com

1015-8987/12/0294-0583$38.00/0

Accessible online at:
www.karger.com/cpb

Xue-Jun Li, Professor
Department of Pharmacology, School of Basic Medical Science
Peking University, 38 Xueyuan Road, Beijing, 100191 (P.R. China)
Tel. +8610 82802863, Fax +8610 82802863
E-Mail xjli@bjmu.edu.cn

response, decreased quantity of granulation tissue, peripheral neuropathy and reduced wound angiogenesis [3, 4]. Oxidative stress has been proposed as an important pathogenic factor in diabetic wound complications [5]. Sustained hyperglycemia-mediated superoxide anion ($O_2^{\cdot-}$) overproduction, which is the main initiator of oxidative stress, leads to the activation of several pathways involved in the pathogenesis of diabetic wound healing, including stimulation of the polyol and glucosamine pathways, activation of protein kinase C, formation of advanced glycation end products (AGEs) [6]. Through these pathways, increased intracellular reactive oxygen species (ROS) cause defective angiogenesis in response to ischemia and activate a number of proinflammatory pathways [5]. Several lines of evidence indicate that mitochondria are a major source of cellular ROS in diabetes [7]. Accordingly, our previous study demonstrated that cutaneous gene therapy of mitochondrial antioxidant enzyme manganese superoxide dismutase (MnSOD) was able to restore the delayed diabetic wound healing with suppression of wound $O_2^{\cdot-}$, as well as a concomitant augmentation of nitric oxide (NO) level [8, 9].

Ganoderma lucidum (Leyss. ex Fr.) Karst. (Lingzhi), one of the most popular medicinal fungi with a long history in oriental countries, has been extensively used in the treatment of a variety of diseases including cancer, hyperlipidemia, diabetes, neurasthenia, insomnia, hypertension and chronic hepatopathy [10, 11]. *Ganoderma lucidum* polysaccharide (*Gl*-PS), a glycopeptide isolated from the water-soluble polysaccharides of *Ganoderma lucidum*, is the primary effective component of *Ganoderma lucidum* [12-14]. Our and some others' previous studies have demonstrated that *Gl*-PS administration significantly prevented the progression of diabetic renal complications and attenuated myocardial collagen cross-linking and AGEs in diabetic rats, by exerting greater antioxidative activity [15, 16]. Moreover, *Gl*-PS could significantly reduce malondialdehyde (MDA) content and ROS production and increase the MnSOD activity both *in vivo* and *in vitro* [17, 18].

Therefore, in the present study, we tested the hypothesis that *Gl*-PS could promote diabetic wound healing and identified underlying mechanisms by using full-thickness excisional wound and streptozotocin (STZ)-induced type 1 diabetic mice. Our results demonstrated that *Gl*-PS could rescue the delayed wound healing in diabeteic mice, through enhancing MnSOD activity, wound angiogenesis and NO level and suppressing mitochondrial oxidative stress.

Materials and Methods

Preparation of Gl-PS

Ganoderma lucidum (Leyss. ex Fr.) Karst was collected in Fujian province, China. The fruiting body of *Ganoderma lucidum* (Leyss. ex Fr.) Karst was authenticated by Prof. MAO Xiaolan, Institute of Microbiology of Chinese Academy of Science. *Gl*-PS was extracted by hot water from the fruiting body of *Ganoderma lucidum* (Leyss. ex Fr.) Karst, followed by ethanol precipitation, reserve dialysis and protein depletion as previously described [19]. The yield of *Gl*-PS was 0.82% (w/w) in terms of the fruiting body of *Ganoderma lucidum*. The component sugar and molecular weight distribution of the glycopeptides were determined by gel permeation chromatography (GPC) and high performance liquid chromatography (HPLC). The structure of the glycopeptides was detected by IR, ^{1}HNMR and ^{13}CNMR. It is a polysaccharide peptide with a molecular weight of 584,900 and has 17 amino acids. The ratio of polysaccharide to peptides is 93.51%: 6.49%. The polysaccharide consists of rhamnose, xylose, fructose, galactose, mannose and glucose with molar ratios of 0.793: 0.964: 2.944: 0.167: 0.384: 7.94 and is linked by h-glycosidic linkages. It is a hazel-colored and water-soluble powder.

Animals

All procedures involving animals were conducted in accordance with the European Community guidelines for the use of experimental animals and approved by the Peking University Committee on Animal Care and Use. C57BL/6 male mice at 10-12 weeks of age (20-25 g, purchased from the Animal Center of Peking University, Beijing) were rendered diabetic by intraperitoneal (i.p.) injection of 60 mg/kg STZ (Sigma-Aldrich, St Louis, MO, USA) in 50 mM sodium citrate (pH 4.5) daily for 5 days, as previously described [9]. Control mice were treated with daily injection of citrate buffer. Blood glucose was measured from the mouse tail vein using an ACCU-CHEK Aviva blood glucose monitor (Roche, Mannheim, Germany). Once blood glucose level reached above 250 mg/dL, daily measurements followed for 1 week prior to experiments [20].

Full thickness excisional wound and drug administration

A full thickness excisional wound was created as previously described [9]. Briefly, one week after blood glucose reached 250 mg/dL, mice were anesthetized with a halothane/oxygen vapor mixture (1.0-1.5%), and the dorsum was clipped free of hair. Full-thickness skin was removed on the dorso-medial back of each animal using a 4-mm punch biopsy (Acuderm inc., Fort Lauderdale, FL, USA), exposing the underlying muscle, and then the wound was covered with a bioclusive transparent dressing (Johnson & Johnson, Milpitas, CA, USA). Wound closure rate was measured by tracing the wound area every other day onto the bioclusive dressing. Tracings were digitized, and areas were calculated in blinded fashion with the use of a computerized algorithm (Image-pro plus 5.0; Media Cybernetics, Inc., Silver Spring, MD, USA). Diabetic mice were divided into four groups and were

respectively given intragastrically 10, 50 and 250 mg/kg of *Gl*-PS or *Gl*-PS vehicle (i.e. distilled water) once daily since the date of wounding. Non-diabetic control received distilled water intragastrically.

Laser Doppler perfusion imaging

Tissue blood flow in regions of the dorsum wound area was measured by using a laser Doppler perfusion imager (MoorLDI, Moor Instruments Ltd, Devon, UK) on days 2, 4, 6 and 8 after surgery. This relative measure of volume flow is expressed in arbitrary perfusion units (PU). The recorded images were analyzed using dedicated software (MoorLDI v2.1; Moor Instruments Ltd, Devon, UK) and the perfusion value was taken and divided by the baseline measurement to give a ratio representing the change in flow.

Superoxide and mitochondrial superoxide measurement

The superoxide-sensitive fluorescent dye dihydroethidium (DHE) was used to evaluate *in situ* production of $O_2^{\cdot-}$ on wound closure as described [9]. Unfixed frozen skin tissues were cut into 30-µm sections and placed on glass slides. Slides were incubated with 1 µM DHE (Invitrogen, Carlsbad, CA, USA) in a light-protected, humidified chamber at 37°C for 30 minutes and then coverslipped. Mitochondrial superoxide was measured using the fluorogenic probe MitoSOX Red (Invitrogen, Carlsbad, CA, USA). Slides were incubated with 5 µM MitoSOX Red at 37°C for 10 minutes and then coverslipped. Fluorescence images were immediately captured with an inverted microscope (1X2-ILL100; Olympus, Tokyo, Japan). Images were collected and stored digitally.

Lipid peroxide measurement

Lipid peroxide was determined by measuring MDA in the skin homogenate. Skin tissues were homogenized in lysis buffer (1% Triton-X100, 50 mM Tris-HCl (pH 8.0), 0.25 M NaCl, 5 mM EDTA, 1:4 (w/v)), homogenates were centrifuged (12, 000 g for 15 minutes, 4°C) and protein supernatants were measured. The lipid peroxide level was established spectrophotometrically at 532 nm by thiobarbituric acid test, as the extinction coefficient and was expressed as µM MDA/mg protein [21].

Nitrite measurement

Wound tissues were cut into small pieces on wound closure and used to determine the nitrite level with the NO assay kit (Keygen, Nanjing, China). After incubation with Eagle's minimal essential medium (EMEM) in a CO_2 incubator for 24 hours, wound tissues were weighed, and the NO stable metabolite nitrite concentration in EMEM was determined [8]. The absorbance at 540 nm was measured with a microplate reader (Thermomax, Molecular Devices Corp., Menlo Park, CA, USA). The concentrations of nitrite were calculated following the instruction of the kit.

NOS activity assay

Skin tissues were homogenized and centrifuged, and supernatants were subjected to NOS activity assay with a commercial NOS assay kit (Keygen, Nanjing, China). Briefly, aliquots of supernatants were incubated with the working solution supplied in the kit, and after incubation at 37°C for 15 min the reaction was terminated by adding the terminating solution provided in the kit. The absorbance was determined using the spectrophotometer at 530 nm. Constitutive NOS (eNOS and neuronal NOS) activity was determined by taking the difference between total NOS activity and inducible nitric oxide synthase (iNOS) activity, as we previously described [9]. Results were normalized to protein content as measured by the bicinchoninic acid (BCA) assay (Thermo Scientific Pierce, Rockford, IL, USA).

MnSOD and CuZnSOD activity assay

MnSOD and copper-zinc superoxide dismutase (CuZnSOD) activity in skin was measured as described previously [8, 22] with minor modification. Briefly, Skin tissues were homogenized in cold lysis buffer mentioned above, and homogenates were centrifuged at 12,000 g for 15 minutes at 4°C. To separate mitochondrial MnSOD from cytosolic CuZnSOD, protein supernatants were treated with CuZnSOD inhibitor and subjected to a commercial superoxide dismutase (SOD) assay kit (Beyotime Institute of Biotechnology, Jiangsu, China).

Catalase activity assay

To examine the catalase specific activity, skin tissues were homogenized in cold lysis buffer mentioned above, and homogenates were centrifuged at 12,000 g for 15 minutes at 4°C. Catalase activity was assayed according to a commercial catalase assay kit (Beyotime Institute of Biotechnology, Jiangsu, China).

Glutathione and GPx measurement

For the total glutathione content and glutathione peroxidase (GPx) assay, skin tissues were homogenized in cold lysis buffer mentioned above, and homogenates were centrifuged at 12,000 g for 15 minutes at 4°C. Glutathione content and GPx activity in the supernatants were analyzed according to the manufacturer's manual (Beyotime Institute of Biotechnology, Jiangsu, China).

Immunoprecipitation assays

Solubilized isolated proteins (250 µg) were resuspended in 200 µl of RIPA buffer (9.1 mM Na_2HPO_4, 1.7 mM NaH_2PO_4, 150 mM NaCl, 0.5% sodium deoxycholate, 1% v/v Nonidet P40, 0.1% SDS, pH 7.2) [23]. Polyclonal anti-MnSOD antibody (Santa Cruz Biotechnology, Santa Cruz, CA, USA) was added and incubated overnight at 4°C. Immune complexes were precipitated with 20 µl protein A/G-Agarose (Santa Cruz Biotechnology, Santa Cruz, CA, USA) and collected by centrifugation at 1,000 g for 5 min at 4°C, and then washed four times with RIPA buffer. Immunoprecipitated samples were recovered by resuspending in 2x sample loading buffer, heated in boiling water for 5 min, and immediately fractionated by reducing sodium dodecyl sulfate-polyacrylamide gel electrophoresis (SDS–PAGE), and the sample was incubated with 10 µg/ml IgG as negative control. Nitration of MnSOD was detected by chemiluminescence (ECL) detection kit (Santa Cruz Biotechnology, Santa Cruz, CA, USA) and

	Control (n = 9-16)	Diabetic (n = 14)	Diabetic + 10 mg/kg *Gl*-PS (n = 8-14)	Diabetic + 50 mg/kg *Gl*-PS (n = 9-12)	Diabetic + 250 mg/kg *Gl*-PS (n = 8-12)
Body weight (g)					
Before treatment	24.72 ± 0.28	22.60 ± 0.73*	22.04 ± 0.70**	21.87 ± 0.87*	22.08 ± 0.61**
After treatment	25.68 ± 0.36	21.44 ± 0.80***	21.66 ±1.05*	21.10 ± 0.81***	22.56 ± 0.56**
Blood glucose levels (mg/dL)					
Before treatment	165.60 ± 9.30	418.10 ± 18.37***	428.40 ± 22.93***	421.70 ± 30.68***	423.60 ± 22.89***
After treatment	169.10 ± 6.56	415.00 ± 21.57***	405.00 ± 32.44***	402.40 ± 19.90***	412.70 ± 17.01***

Table 1. General characteristics of mice following Gl-PS treatment. Diabetic status induced by daily injection of streptozotocin for 5 days (60 mg/kg i.p.) in mice, control mice were treated with daily injections of citrate buffer. Values were mean ± SEM ($^{*}P$<0.05, $^{**}P$<0.01,$^{***}P$<0.001, compared with the normal control group)

evaluated by densitometric image analysis with Quantity One software version 4.4.0 (Bio-Rad Laboratories, Hercules, CA, USA).

Immunoblot analysis

Briefly, skin tissues were homogenized in lysis buffer (1% Triton-X100, 50 mM Tris-HCl (pH 8.0), 0.25 M NaCl, 5 mM EDTA) with a mixture of protease inhibitors (Calbiochem, San Diego, CA, USA). Homogenates were centrifuged (12,000 g for 15 minutes, 4°C), and protein supernatants were measured using the BCA method. Equal amounts of protein were analyzed by using 12% SDS–PAGE and electrophoretically transferred onto polyvinylidene difluoride (PVDF) immobilion-P membranes of 0.45-µm pore size (Millipore Corp, Bedford, MA, USA). Membranes were blocked in blocking buffer (phosphate-buffered saline plus 0.05% Tween-20 and 5% non-fat dry milk) for 1 h or more, and then incubated overnight at 4°C with following antibodies. Mouse anti-nitrotyrosine (1/200) (Cayman Chemicals, Ann Arbor, MI, USA), rabbit anti-MnSOD (1/1,000) (Santa Cruz Biotechnology, Santa Cruz, CA, USA), mouse anti-p66Shc (1/1,000) (BD Biosciences, Franklin Lakes, NJ, USA), mouse anti-p66Shc phosphorylated at Ser^{36} (1/200) (Axxora Platform, San Diego, CA, USA), rabbit anti-Pin1 (1/1,000) (Cell Signaling Technology, Beverly, MA, USA), mouse anti-glyceraldehyde-3-phosphate dehydrogenase (GAPDH) (1/10,000) (Sigma-Aldrich, St Louis, MO, USA). After incubation with the appropriate horseradish peroxidase-conjugated secondary antibody, blots were developed using an enhanced ECL detection kit. The staining intensity of the bands was determined by densitometric image analysis.

Statistical analysis

Data were expressed as means ± SEM. The significance of differences between groups was evaluated by unpaired Student's t-test. When >2 treatment groups were compared, one-way ANOVA with Newman-Keuls test was used. A probability level of P<0.05 was considered statistically significant.

Results

Induction of diabetes in mice

As shown in Table 1, STZ administration-induced diabetes in mice was shown by hyperglycemia (blood glucose levels: 415.00 ± 21.57 vs. 169.10 ± 6.56 mg/dL in normal control mice, P<0.001). Diabetes also resulted in a highly significant impairment of body weight gain (21.44 ± 0.80 vs. 25.68 ± 0.36 g in normal control mice, P<0.001). *Gl*-PS treatment at dose of 10, 50 mg/kg and 250 mg/kg did not significantly modify either blood glucose or body weight.

Effects of Gl-PS on wound healing in diabetic mice

As shown in Fig. 1A, compared with control mice, the rate of wound closure was significantly delayed in diabetic mice (39.51 ± 3.72% vs. 68.40 ± 2.36% on day 6, P<0.01). *Gl*-PS administration (250 mg/kg) to diabetic mice significantly accelerated the rate of wound closure by as much as 2 days and continued through day 14. The percentage of wound closure on day 6 in diabetic mice treated with 250 mg/kg *Gl*-PS was significantly higher than that of diabetic control mice (61.34 ± 7.06% vs. 39.51 ± 3.72% on day 6, P<0.05) (Figs. 1B, 1C). There was significant difference in wound healing between diabetic mice treatment with *Gl*-PS at dose of 50 mg/kg and diabetic control mice except on day 2 and 6 (51.76 ± 8.01 vs. 39.51 ± 3.72% on day 6, P>0.05). There was no significant difference in wound healing between diabetic mice treatment with *Gl*-PS at dose of 10 mg/kg and diabetic control mice except on day 2, 8 and 14 (50.08 ± 3033 vs. 39.51 ± 3.72% on day 6, P>0.05).

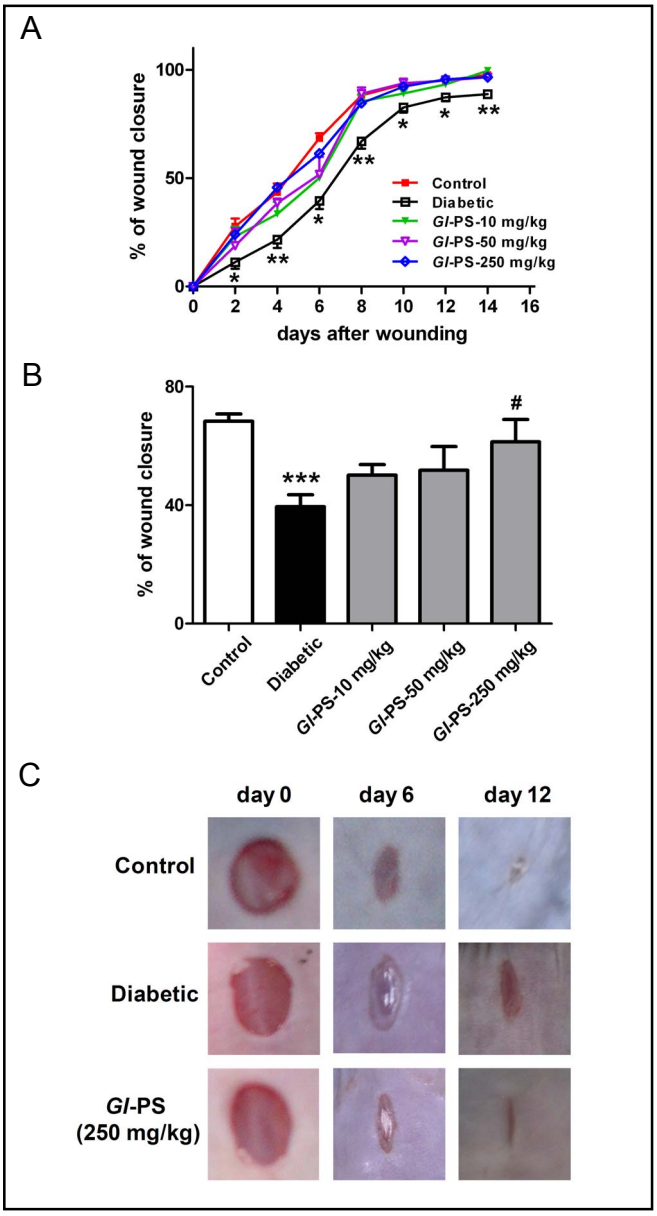

Fig. 1. (A) Wound closure rate in control, diabetic mice and diabetic mice treated with 10, 50 and 250 mg/kg *Gl*-PS. Data were expressed as mean ± SEM. n = 5-14 for each time period. $^{*}P<0.05$, $^{**}P<0.01$ vs. control mice. (B) Wound closure rate in control, diabetic mice and diabetic mice treated with *Gl*-PS on day 6. Data were expressed as mean ± SEM. n= 7-11 per group. $^{***}P<0.001$ vs. control mice, $^{\#}P<0.05$ vs. diabetic mice. (C) Representative wounds on day 0, 6, 12 after injury were shown for each group.

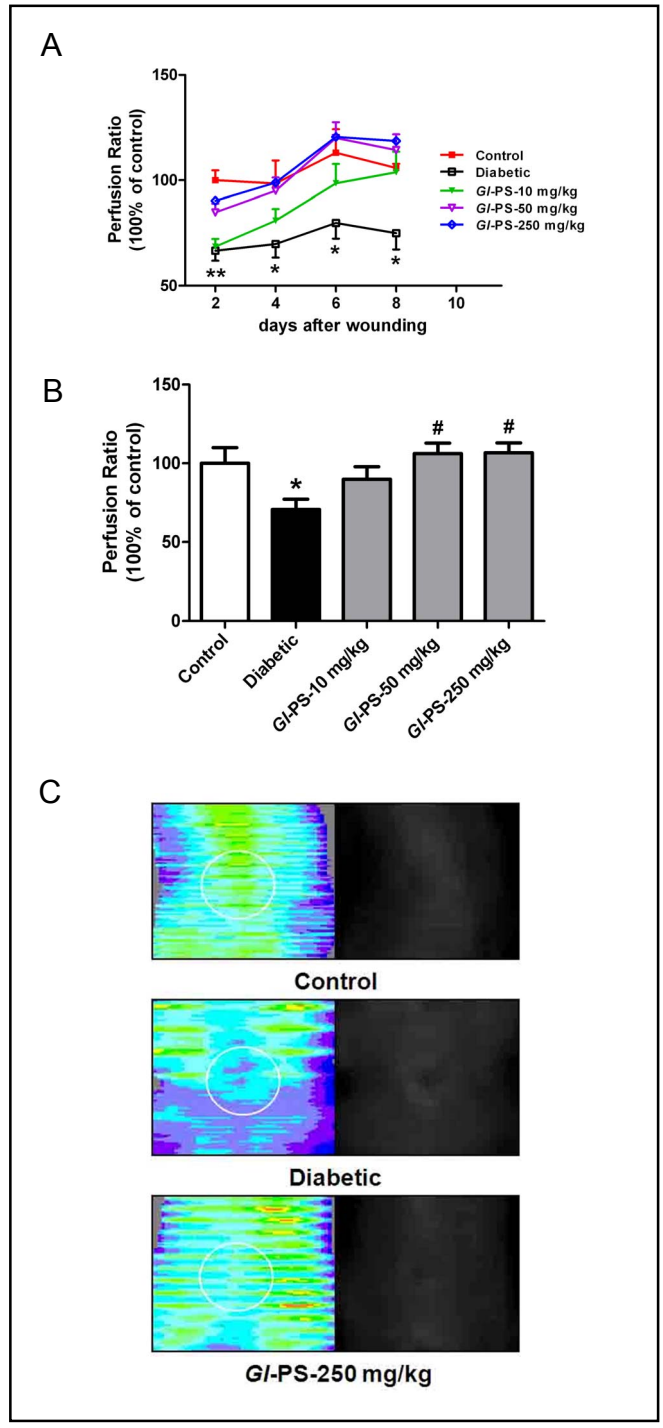

Fig. 2. (A) Wound perfusion in control, diabetic mice and diabetic mice treated with *Gl*-PS on day 2, 4, 6 and 8 was assessed by color laser Doppler. Data were expressed as mean ± SEM. n = 4-14 for each time period. $^{*}P<0.05$, $^{**}P<0.01$ vs. control mice. (B) Wound perfusion in control, diabetic mice and diabetic mice treated with *Gl*-PS on day 6. Data were expressed as mean ± SEM. n = 8-14 per group. $^{*}P<0.05$ vs. control mice, $^{\#}P<0.05$ vs. diabetic mice. (C) Color scale illustrated variations in blood flow from high flow (bright pixels) to minimal flow (dark pixels), wound area was circled. Phase-contrast images showed the morphology of wound.

Effects of Gl-PS on perfusion around the wound in diabetic mice

The mean perfusion rate around the wound was analyzed by using laser Doppler perfusion imager at days 2, 4, 6, and 8 after surgery (Fig. 2A). The mean perfusion rate was steadily increased and peaked on day 6, then plateaued and started declining in different groups.

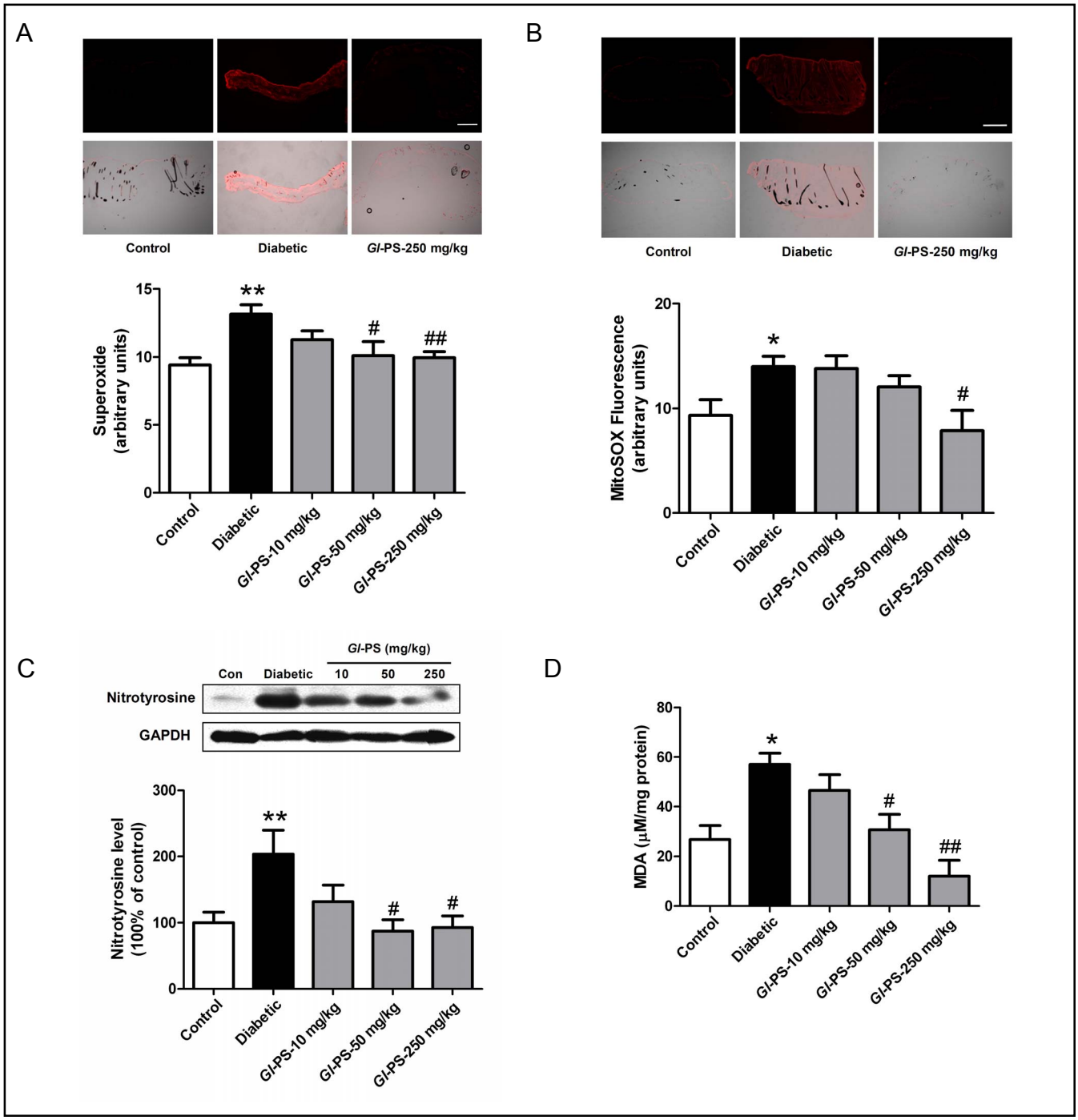

Fig. 3. (A) Effect of *Gl*-PS on cutaneous $O_2^{\cdot-}$ production in diabetic mice. Representative sections of skin tissue (30 μm) were shown; top, fluorescence image, bottom, fluorescence image superimposed with transmittal image. Statistical data of fluorescence measurement were presented as histograms in the bottom panels. Data were expressed as mean ± SEM. n=6-13 per group. $^{*}P<0.05$ vs. control mice, $^{\#}P<0.05$, $^{\#\#}P<0.01$ vs. diabetic mice. Bar=100 μm. (B) Effect of *Gl*-PS on cutaneous mitochondrial $O_2^{\cdot-}$ level in diabetic mice. Representative sections of skin tissue (30 μm) were shown, top, fluorescence image; bottom, fluorescence image superimposed with transmittal image. Statistical data of fluorescence measurement were presented as histograms in the bottom panels. Data were expressed as mean ± SEM. n=6-11 per group. $^{*}P<0.05$ vs. control mice, $^{\#}P<0.05$ vs. diabetic mice. Bar=100 μm. (C) Effect of *Gl*-PS on cutaneous nitrotyrosine formation in diabetic mice. Cutaneous nitrotyrosine was analyzed by Western Blot. Immunoblots of representative samples were shown, statistical data were shown as histograms at the bottom panels. Data were expressed as mean ± SEM and were shown as a percentage of the control. n=6-12 per group. $^{**}P<0.01$ vs. control mice, $^{\#}P<0.05$ vs. diabetic mice. (D) Effect of *Gl*-PS on cutaneous MDA concentrations in diabetic mice. Data were expressed as mean ± SEM. n=5-13 per group. $^{*}P<0.05$ vs. control mice, $^{\#}P<0.05$, $^{\#\#}P<0.01$ vs. diabetic mice.

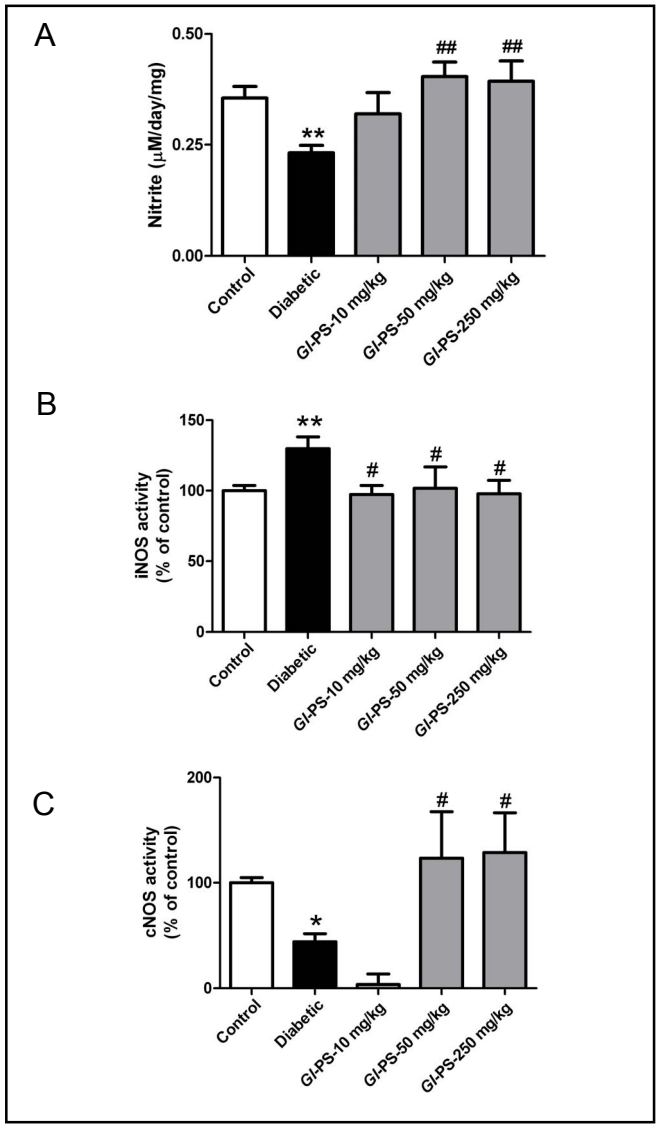

Fig. 4. (A) Cutaneous nitrite level on wound closure in control, diabetic mice and diabetic mice treated with *Gl*-PS. Data were expressed as mean ± SEM. n = 4-14 per group. $^{**}P<0.01$ vs. control mice, $^{\#\#}P<0.01$ vs. diabetic mice. (B) Effect of *Gl*-PS on cutaneous iNOS activity in diabetic mice. Data were expressed as mean ± SEM. n=6-11 per group. $^{**}P<0.01$ vs. control mice, $^{\#}P<0.05$ vs. diabetic mice. (C) Effect of *Gl*-PS on cutaneous cNOS activity. Data were expressed as mean ± SEM. n=5-11 per group. $^{*}P<0.05$ vs. control mice, $^{\#}P<0.05$ vs. diabetic mice.

Compared with control mice, the mean perfusion rate was significantly decreased at day 2 and continued through day 8 in diabetic mice (100.00 ± 9.92 vs. 70.63 ± 6.60 on day 6, $P<0.05$). 250 mg/kg *Gl*-PS treatment significantly increased the mean perfusion rate on day 2, 4, 6 and 8 in diabetic mice (106.70 ± 6.20 vs. 70.63 ± 6.60 on day 6, $P<0.05$) (Fig. 2A). 50 mg/kg *Gl*-PS treatment induced an upregulation of the mean perfusion rate on day 4, 6 and 8 in diabetic mice (106.20 ± 6.67 vs. 70.63 ± 6.60 on day 6, $P<0.05$). There was no significant difference in the mean perfusion rate between diabetic mice treatment with *Gl*-PS at dose of 10 mg/kg and diabetic control mice (89.87 ± 8.00 vs. 70.63 ± 6.60 on day 6, $P>0.05$) (Figs. 2B, 2C).

Effects of Gl-PS on cutaneous $O_2^{\cdot-}$ and mitochondrial $O^{\cdot}_2^{-}$ level in diabetic mice

To determine the effect of *Gl*-PS on cutaneous oxidative stress in diabetes, we estimated cutaneous $O_2^{\cdot-}$ and mitochondrial $O_2^{\cdot-}$ level. In situ detection of $O_2^{\cdot-}$ by DHE staining showed that cutaneous $O_2^{\cdot-}$ level in untreated diabetic mice was increased compared to control mice ($P<0.05$) (Fig. 3A). Cutaneous $O_2^{\cdot-}$ level in diabetic mice treatment with *Gl*-PS was significantly attenuated compared with that of untreated diabetic mice (Fig. 3A). Consistently, MitoSOX Red staining revealed that increased cutaneous mitochondrial $O_2^{\cdot-}$ level in diabetic mice was diminished by *Gl*-PS treatment (Fig. 3B).

Effects of Gl-PS on cutaneous nitrotyrosine formation and MDA level in diabetic mice

Excessive production of $O_2^{\cdot-}$ is known to rapidly react with NO to form the stable peroxynitrite anion ($ONOO^-$) which is highly toxic and thought to be principal mediators of oxidative cellular damage [23]. Cutaneous $ONOO^-$ formation was determined by using nitrotyrosine antibodies. As shown in Fig. 3C, nitrotyrosine was detected mainly in the protein bands of 55 kDa in skin and levels of nitrotyrosine increased dramatically in untreated diabetic mice skin. 50 and 250 mg/kg *Gl*-PS treatment significantly suppressed nitrotyrosine formation in diabetic mice skin. Moreover, 50 and 250 mg/kg *Gl*-PS administration dose-dependently attenuated MDA concentrations, a lipid peroxidation index, in diabetic mice skin (Fig. 3D).

Effects of Gl-PS on nitrite level and NOS activity in diabetic mice

Cutaneous NO level was estimated by measuring its stable metabolite nitrite. Cutaneous nitrite level was significantly reduced in untreated diabetic mice compared to the non-diabetic controls. 50 and 250 mg/kg *Gl*-PS administration resulted in a significant increase of cutaneous nitrite level in diabetic mice compared to untreated diabetic mice ($P<0.05$) (Fig. 4A).

We further evaluate whether cNOS and iNOS activities were altered by *Gl*-PS treatment. In untreated diabetic mice, cutaneous cNOS activity was decreased,

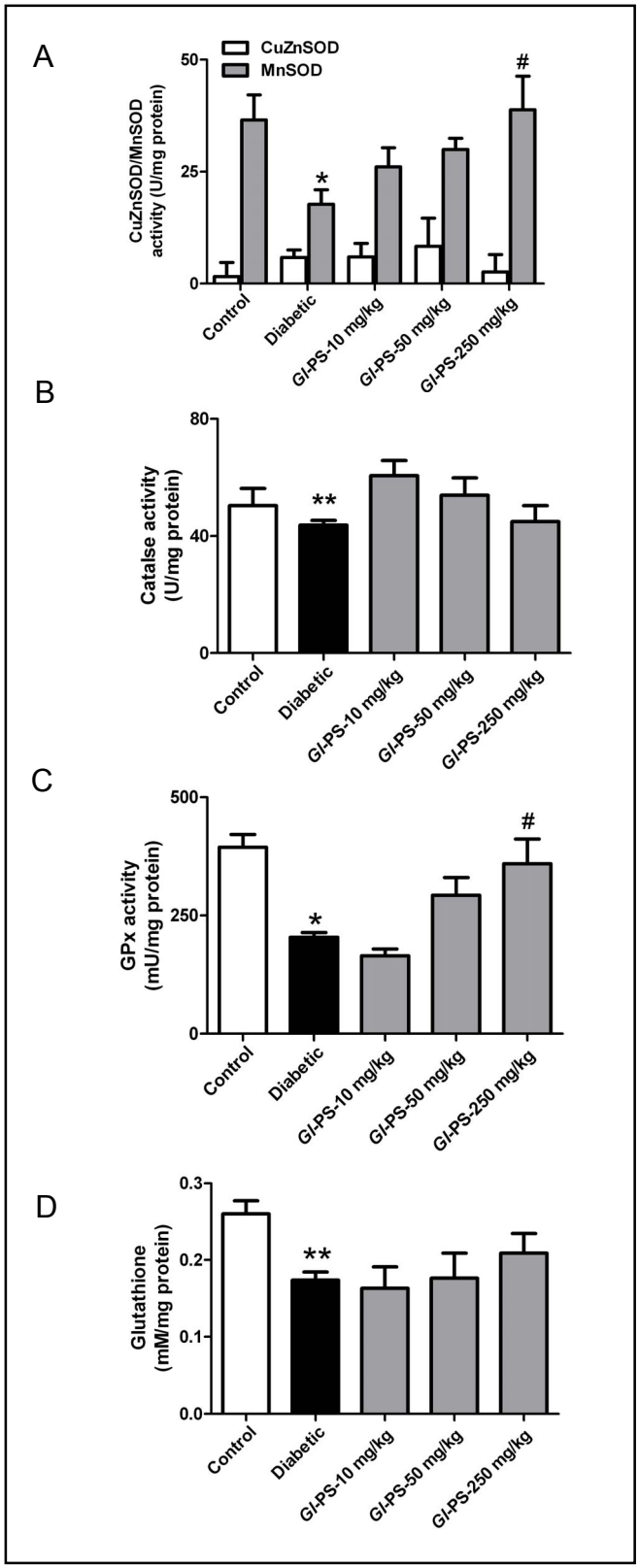

Fig. 5. Effects of *Gl*-PS on cutaneous MnSOD, CuZnSOD (A), catalase (B), GPx (C) activity and total glutathione content (D) in diabetic mice. Data were expressed as mean ± SEM. n=4-10 per group. $^{*}P<0.05$, $^{**}P<0.01$ vs. control mice, $^{\#}P<0.05$ vs. diabetic mice.

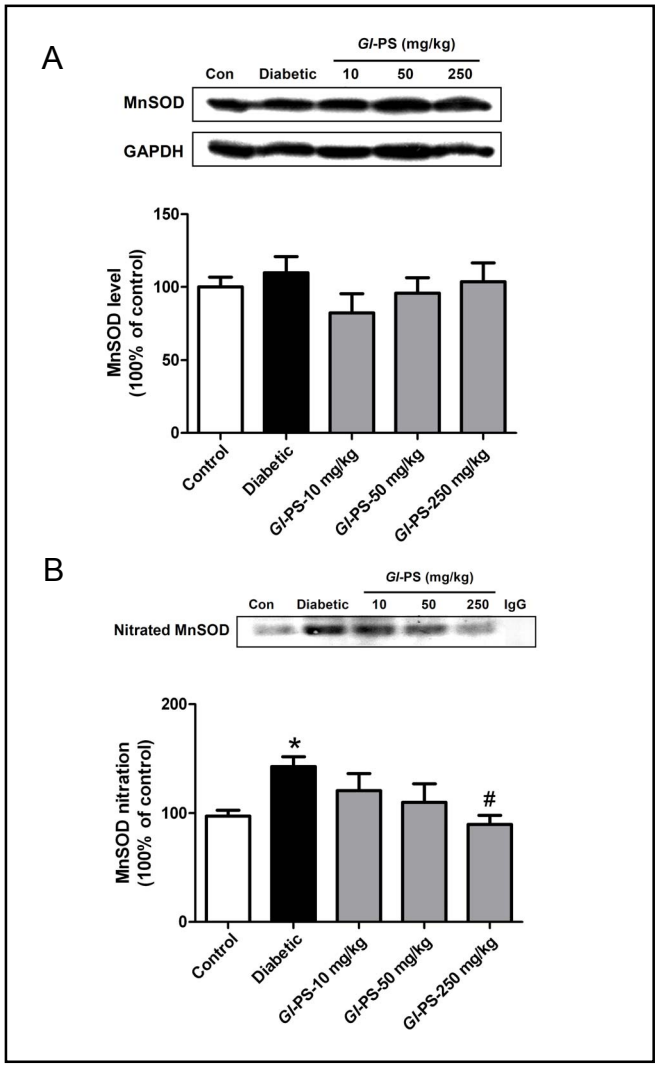

Fig. 6. (A) Effect of *Gl*-PS on MnSOD protein expression in diabetic mice skin. Cutaneous MnSOD was analyzed by Western Blot. Immunoblots of representative samples were shown, statistical data were shown as histograms at the bottom panels. Data were expressed as mean ± SEM and were shown as a percentage of the control. n=5-12 per group. (B) Effect of *Gl*-PS on MnSOD nitration in diabetic mice skin. Proteins extracted from skin homogenates were immunoprecipitated with anti-MnSOD antibody and resolved in 12% SDS–PAGE followed by Western Blot analysis with the antibody against nitrotyrosine. Immunoblots of representative samples were shown, statistical data were shown as histograms at the bottom panels. Data were expressed as mean ± SEM and were shown as a percentage of the control. n=4-6 per group. $^{*}P<0.05$ vs. control mice, $^{\#}P<0.05$ vs. diabetic mice.

in contrast, iNOS activity was significantly increased. *Gl*-PS treatment markedly suppressed iNOS activity in diabetic mice, and 50 and 250 mg/kg *Gl*-PS administration leaded to augment of cNOS activity (Figs. 4B, 4C).

Effects of Gl-PS on cutaneous MnSOD/ CuZnSOD, catalase and GPx activities *and glutathione level in diabetic mice*

SODs constitute the first defense step by preventing superoxide anion from forming singlet oxygen. To understand the mechanism underlying the protective effect of *Gl*-PS, changes in activities of SODs, GPx and catalase and total glutathione content were investigated. As shown in Fig. 5A, diabetic mice had lower MnSOD activity, *Gl*-PS administration markedly enhanced MnSOD activity in diabetic mice in a dose-dependent manner, while it did not modify activities of CuZnSOD. GPx (Fig. 5C) and catalase (Fig. 5B) activities in diabetic mice were significantly reduced as compared with non-diabetic control animals; *Gl*-PS treatment restored GPx activity but it did not modify the decrease of catalase activity in diabetic mice skin. Furthermore, total glutathione content was significantly decreased in the skin of diabetic mice, *Gl*-PS administration resulted in a higher level but no obvious differences in the total glutathione content (Fig. 5D).

Effects of Gl-PS on MnSOD nitration/ inactivation in diabetic mice

We next estimated whether MnSOD protein level was altered by *Gl*-PS treatment. MnSOD protein expression level was the same in different group (Fig. 6A). Intracellular peroxynitrite could promote nitration of tyrosine residues on proteins; MnSOD, one of the targets of tyrosine nitration, could be inactivated by peroxynitrite [24]. Immunoprecipitation of cellular nitrated MnSOD with anti-MnSOD antibody and anti-nitrotyrosine antibody were used to pull down nitrotyrosine-MnSOD immunocomplex. The immunoprecipitated protein demonstrated an increase of nitrated MnSOD in untreated diabetic mice, and *Gl*-PS treatment alleviated MnSOD nitration in diabetic mice skin (Fig. 6B).

Effects of Gl-PS on cutaneous p66 Shc and Pin1 level in diabetic mice

It has been reported that the adaptor protein p66Shc is implicated in mitochondrial ROS generation. Oxygen-derived free radicals induce Ser^{36} phosphorylation of p66Shc, allowing transfer of the protein from the cytosol to mitochondria via recognition and binding to prolyl-isomerase Pin1. After such mitochondrial internalization, p66Shc inducing ROS generation and apoptosis [25]. In untreated diabetic mice, cutaneous p66Shc, Ser^{36} phosphorylation of p66Shc and Pin1 levels were significantly increased. Treatment with *Gl*-PS suppressed the p66Shc, Ser^{36} phosphorylation of p66Shc and Pin1 levels in a dose-dependent manner (Fig. 7).

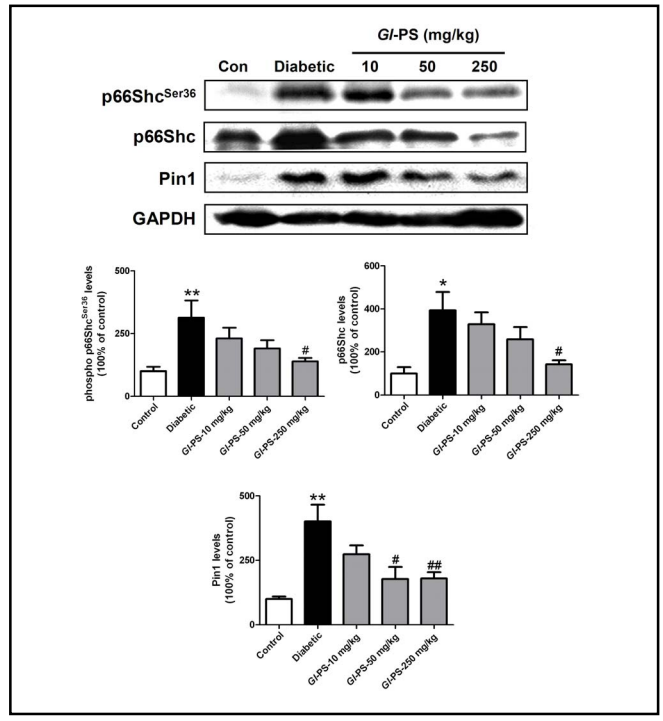

Fig. 7. Effects of *Gl*-PS on cutaneous p66Shc, Ser^{36} phosphorylation of p66Shc and Pin1 levels in diabetic mice. Cutaneous p66Shc, Ser^{36} phosphorylation of p66Shc and Pin1 were analyzed by Western Blot. Immunoblots of representative samples were shown, statistical data were shown as histograms at the bottom panels. Data were expressed as mean ± SEM and were shown as a percentage of the control. n=5-10 per group. $^{*}P<0.05$, $^{**}P<0.01$ vs. control mice, $^{\#}P<0.05$, $^{\#\#}P<0.01$ vs. diabetic mice.

Discussion

The present study provides first evidence that *in vivo Gl*-PS is able to 1) ameliorate the wound healing delay and increase perfusion around the wound in STZ-induced type 1 diabetic mice, 2) significantly increase cutaneous NO, decrease mitochondrial $O_2^{\cdot -}$ production, and potentiate cutaneous MnSOD activity, 3) significantly normalize p66Shc, phosphorylation of p66Shc at Ser^{36} and Pin1.

Our and some others' previous studies have demonstrated that *Gl*-PS has hypoglycemic activity by increasing plasma insulin both in STZ and alloxan-induced diabetic mice [26, 27]. However, our current result suggested that *Gl*-PS treatment could not reverse STZ induced glucose increase and body weight loss in STZ-

induced type 1 diabetic mice. The results confirm our previous findings showing that pre-treatment of islets with *Gl*-PS potentiated alloxan-induced islets viability loss and inhibited free radicals production, whereas simultaneous addition of *Gl*-PS with alloxan could not prevent islet cells from being destroyed [26]. In addition, we have proved that *Gl*-PS pre-treatment up-regulated the glucose transporter 2 (GLUT2) protein expression in pancreatic islets of STZ-induced diabetic mice [10, 28]. Therefore, the pre-treatment of *Gl*-PS is required for protection of pancreatic islets against cytotoxicity.

Overproduction of superoxide is the first and key event in the activation of all other pathways involved in the pathogenesis of diabetes complications [29]. Excessive $O_2^{\cdot-}$ generation leads to the intracellular depletion of tetrahydrobiopterin (BH4), which is the essential cofactor for activity of all NOS enzymes. Reduced level of BH4 results in NOS uncoupling and the consequent production of $O_2^{\cdot-}$ instead of NO [30]. In the current study, *Gl*-PS treatment markedly suppressed iNOS activity and normalized both $O_2^{\cdot-}$ production and nitrotyrosine formation in diabetic mice. Compared with cutaneous cNOS activity, iNOS activity was enhanced in diabetic mice, indicating that iNOS uncoupling was critical to $O_2^{\cdot-}$ production. In support of this view, we have demonstrated that iNOS inhibition could also ameliorate impaired wound healing and attenuated cutaneous $O_2^{\cdot-}$ production and nitrotyrosine formation in diabetic mice (unpublished). Moreover, *Gl*-PS has been proved to be able to inhibit iNOS protein expression in BCG-induced hepatic damage in mice and *Ganoderma lucidum* could inhibit iNOS expression in macrophages [31, 32]. Presumably more NO formation via iNOS leads to elevated peroxynitrite formation. Here, we provide evidence that iNOS did not contribute to the nitrite formation, the surrogate marker of NO. *Gl*-PS administration evoked a significant increase of cutaneous nitrite level in diabetic mice with the inhibition of iNOS activity. In support of this possibility, by using the superoxide spin trap DEPMPO and the NO spin trap Fe-MGD complex, Huisman proved that BH4 cofactor-deficient iNOS is not a NO-producing enzyme, but a superoxide-producing enzyme [33].

Mitochondria are a main source of ROS in cells. Mitochondrial dysfunction increases electron leak and the generation of ROS from the mitochondrial respiratory chain (MRC) [34] The redox enzyme p66Shc, which localizes within the mitochondrial intermembrane space, produces approximately one third of the total intracellular hydrogen peroxide (H_2O_2) pool [25]. It has been reported that p66Shc protein is up-regulated in aortas of diabetic

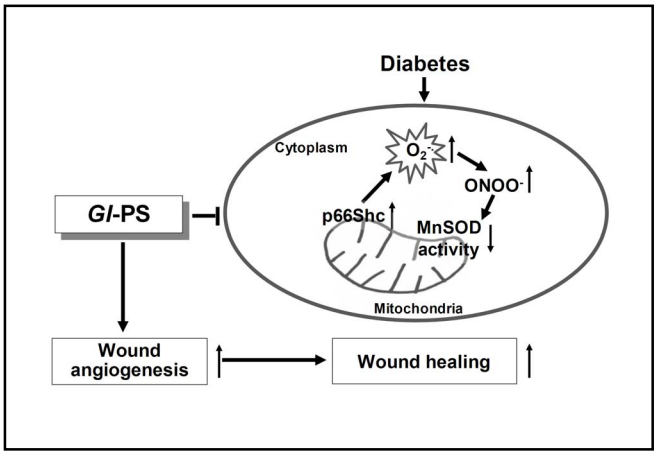

Fig. 8. Schematic illustration of possible mechanisms on *Gl*-PS regulation of oxidative stress and wound healing in type 1 diabetes. *Gl*-PS ameliorated the wound healing delay by decreasing cutaneous $O_2^{\cdot-}$ production and nitrotyrosine formation and increasing MnSOD activation and wound angiogenesis. In addition, *Gl*-PS inhibited p66Shc expression level in cutaneous tissue of diabetic mice.

mice; deletion of p66Shc could protect diabetic mice from hyperglycemia-induced, $ONOO^-$ generation, lipid peroxidation and endothelial dysfunction [35]. In this study, we showed consistently that *Gl*-PS administration led to the inhibition of both p66Shc expression level and oxidative stress in a dose-dependent manner. Fadini and Albiero [6] demonstrated that diabetic delayed wound healing was significantly improved in p66Shc knockout mice as compared with wild type mice. Pinton and Rimessi [36] demonstrated that under oxidative conditions activated protein kinase C-β could induce Ser^{36} phosphorylation of p66Shc and trigger its mitochondrial accumulation after it being recognized and binding to the prolyl isomerase Pin1. In light of their report, our results show that *Gl*-PS treatment suppressed both Ser^{36} phosphorylation of p66Shc and Pin1 levels, which indicates that *Gl*-PS may prevent the accumulation of p66Shc in mitochondria. In addition, Francia and delli Gatti [37] demonstrated that iNOS was up-regulated in aortas of old wild type mice with increased $O_2^{\cdot-}$ generation, whereas there were no age-dependent changes in p66Shc knockout mice. Therefore, p66Shc might be the upstream of iNOS. However, we did not address the exact molecular mechanism of p66Shc in regulation of iNOS by *Gl*-PS, which should be proved in the future studies.

It is known that the antioxidant defense system is depleted and that activities of antioxidant enzymes are reduced in diabetics [38]. SODs constitute the first line of defence against ROS. Cytosolic superoxide dismutase

CuZnSOD and mitochondrial superoxide dismutase MnSOD convert intracellular superoxide radicals into hydrogen peroxide which are cleared by GPx and catalase further by converting it into water. However, our current data do not suggest the involvement of *Gl*-PS on the regulation of activities of CuZnSOD and catalase in diabetic mice skin. In support of this possibility, studies from our lab and elsewhere have demonstrated that *Gl*-PS exerted a greater effect on MnSOD others than CuZnSOD [17, 39, 40]. Because of the localization of MnSOD and GPx-1 in the matrix of the mitochondria, in close proximity to the production of ROS by the electron transport chain, these two enzymes are believed to be the primary antioxidant defense systems in the mitochondria [41, 42]. Therefore, we suggested that *Gl*-PS might be a mitochondria-targeted antioxidant. Although expression pattern of MnSOD remained unaltered in different groups, its activity in diabetic mice was significantly reduced compared to normal control, suggesting that the protein was inactivated. Tyrosine nitration of MnSOD was demonstrated more than 10 years ago and it is widely accepted that this modification involves enzymatic inactivation [43]. Moreover, peroxynitrite is the only known biological oxidant competent to inactivate MnSOD enzymatic activity, which has been detected in a number of human and animal models of disease [44]. We now provide evidence for the MnSOD nitration inhibition by *Gl*-PS together with MnSOD enzymatic activation in diabetic wound healing.

Conclusions

The findings of this study demonstrate that *Gl*-PS has ameliorated the wound healing delay in type 1 diabetes via suppressing mitochondrial oxidative stress (Fig. 8). This finding could potentially provide a mechanistic basis for *Gl*-PS as a potential therapeutic strategy to refractory wound healing in diabetes.

Acknowledgements

Gl-PS was kindly provided by Profs. Shu-Qian Lin and Sai-Zhen Wang of Fuzhou Institute of Green Valley Bio-Pharm Technology. This work was supported by the National Natural Science Foundation of China (No. 30901803, 91129727, 81020108031, 30973558, 30572202, 30901815), the Research Fund for the Doctoral Program of Higher Education of China (No. 20090001120046), the Major Specialized Research Fund from the Ministry of Science and Technology in China (No. 2009ZX09103-144) and Research Fund from Ministry of Education of China (111 Projects No.B07001).

References

1 Singer AJ, Clark RA: Cutaneous wound healing. N Engl J Med 1999;341:738-746.

2 Boulton AJ, Vileikyte L, Ragnarson-Tennvall G, Apelqvist J: The global burden of diabetic foot disease. Lancet 2005;366:1719-1724.

3 Brem H, Tomic-Canic M: Cellular and molecular basis of wound healing in diabetes. J Clin Invest 2007;117:1219-1222.

4 Falanga V: Wound healing and its impairment in the diabetic foot. Lancet 2005;366:1736-1743.

5 Giacco F, Brownlee M: Oxidative stress and diabetic complications. Circ Res 2010;107:1058-1070.

6 Fadini GP, Albiero M, Menegazzo L, Boscaro E, Pagnin E, Iori E, Cosma C, Lapolla A, Pengo V, Stendardo M, Agostini C, Pelicci PG, Giorgio M, Avogaro A: The redox enzyme p66shc contributes to diabetes and ischemia-induced delay in cutaneous wound healing. Diabetes 2010;59:2306-2314.

7 Huang C, Kim Y, Caramori ML, Moore JH, Rich SS, Mychaleckyj JC, Walker PC, Mauer M: Diabetic nephropathy is associated with gene expression levels of oxidative phosphorylation and related pathways. Diabetes 2006;55:1826-1831.

8 Luo JD, Wang YY, Fu WL, Wu J, Chen AF: Gene therapy of endothelial nitric oxide synthase and manganese superoxide dismutase restores delayed wound healing in type 1 diabetic mice. Circulation 2004;110:2484-2493.

9 Tie L, Li XJ, Wang X, Channon KM, Chen AF: Endothelium-specific gtp cyclohydrolase i overexpression accelerates refractory wound healing by suppressing oxidative stress in diabetes. Am J Physiol Endocrinol Metab 2009;296:E1423-1429.

10 Lin ZB: Cellular and molecular mechanisms of immuno-modulation by ganoderma lucidum. J Pharmacol Sci 2005;99:144-153.

11 Sanodiya BS, Thakur GS, Baghel RK, Prasad GB, Bisen PS: Ganoderma lucidum: A potent pharmacological macrofungus. Curr Pharm Biotechnol 2009;10:717-742.

12 Wang X, Zhao X, Li D, Lou YQ, Lin ZB, Zhang GL: Effects of ganoderma lucidum polysaccharide on cyp2e1, cyp1a2 and cyp3a activities in bcg-immune hepatic injury in rats. Biol Pharm Bull 2007;30:1702-1706.

13 Zhou ZY, Tang YP, Xiang J, Wua P, Jin HM, Wang Z, Mori M, Cai DF: Neuroprotective effects of water-soluble ganoderma lucidum polysaccharides on cerebral ischemic injury in rats. J Ethnopharmacol 2010;131:154-164.

14 Sun LX, Lin ZB, Li XJ, Li M, Lu J, Duan XS, Ge ZH, Song YX, Xing EH, Li WD: Promoting effects of ganoderma lucidum polysaccharides on b16f10 cells to activate lymphocytes. Basic Clin Pharmacol Toxicol 2011;108:149-154.

15 He CY, Li WD, Guo SX, Lin SQ, Lin ZB: Effect of polysaccharides from ganoderma lucidum on streptozotocin-induced diabetic nephropathy in mice. J Asian Nat Prod Res 2006;8:705-711.
16 Meng GL, Zhu HY, Yang SJ, Wu F, Zheng HH, Chen E, Xu JL: Attenuating effects of ganoderma lucidum polysaccharides on myocardial collagen cross-linking relates to advanced glycation end product and antioxidant enzymes in high-fat-diet and streptozotocin-induced diabetic rats. Carbohyd Polym 2011;84:180-185.
17 Zhao HB, Lin SQ, Liu JH, Lin ZB: Polysaccharide extract isolated from ganoderma lucidum protects rat cerebral cortical neurons from hypoxia/reoxygenation injury. J Pharmacol Sci 2004;95:294-298.
18 Yang Q, Wang S, Xie Y, Sun J, Wang J: Hplc analysis of ganoderma lucidum polysaccharides and its effect on antioxidant enzymes activity and bax, bcl-2 expression. Int J Biol Macromol 2010;46:167-172.
19 Cao LZ, Lin ZB: Regulation on maturation and function of dendritic cells by ganoderma lucidum polysaccharides. Immunol Lett 2002;83:163-169.
20 Gallagher KA, Liu ZJ, Xiao M, Chen H, Goldstein LJ, Buerk DG, Nedeau A, Thom SR, Velazquez OC: Diabetic impairments in no-mediated endothelial progenitor cell mobilization and homing are reversed by hyperoxia and sdf-1 alpha. J Clin Invest 2007;117:1249-1259.
21 Costa B, Trovato AE, Comelli F, Giagnoni G, Colleoni M: The non-psychoactive cannabis constituent cannabidiol is an orally effective therapeutic agent in rat chronic inflammatory and neuropathic pain. Eur J Pharmacol 2007;556:75-83.
22 Marrotte EJ, Chen DD, Hakim JS, Chen AF: Manganese superoxide dismutase expression in endothelial progenitor cells accelerates wound healing in diabetic mice. J Clin Invest 2010;120:4207-4219.
23 Tangpong J, Cole MP, Sultana R, Estus S, Vore M, St Clair W, Ratanachaiyavong S, St Clair DK, Butterfield DA: Adriamycin-mediated nitration of manganese superoxide dismutase in the central nervous system: Insight into the mechanism of chemobrain. J Neurochem 2007;100:191-201.
24 Bayir H, Kagan VE, Clark RS, Janesko-Feldman K, Rafikov R, Huang Z, Zhang X, Vagni V, Billiar TR, Kochanek PM: Neuronal nos-mediated nitration and inactivation of manganese superoxide dismutase in brain after experimental and human brain injury. J Neurochem 2007;101:168-181.
25 Francia P, Cosentino F, Schiavoni M, Huang Y, Perna E, Camici GG, Luscher TF, Volpe M: P66(shc) protein, oxidative stress, and cardiovascular complications of diabetes: The missing link. J Mol Med (Berl) 2009;87:885-891.
26 Zhang HN, He JH, Yuan L, Lin ZB: In vitro and in vivo protective effect of ganoderma lucidum polysaccharides on alloxan-induced pancreatic islets damage. Life Sci 2003;73:2307-2319.
27 Li F, Zhang Y, Zhong Z: Antihyperglycemic effect of ganoderma lucidum polysaccharides on streptozotocin-induced diabetic mice. Int J Mol Sci 2011;12:6135-6145.
28 Zhang HN, Lin ZB: Prevention of low-dose of streptozotocin induced autoimmune diabetic mice with *ganoderma lucidum* polysaccharides. Natl Med J China 2003;83:1999-2000.
29 Ceriello A: Oxidative stress and diabetes-associated complications. Endocr Pract 2006;12:60-62.
30 Channon KM: Tetrahydrobiopterin: Regulator of endothelial nitric oxide synthase in vascular disease. Trends Cardiovasc Med 2004;14:323-327.
31 Zhang GL, Wang YH, Ni W, Teng HL, Lin ZB: Hepatoprotective role of ganoderma lucidum polysaccharide against bcg-induced immune liver injury in mice. World J Gastroenterol 2002;8:728-733.
32 Woo CW, Man RY, Siow YL, Choy PC, Wan EW, Lau CS, O K: Ganoderma lucidum inhibits inducible nitric oxide synthase expression in macrophages. Mol Cell Biochem 2005;275:165-171.
33 Huisman A, Vos I, van Faassen EE, Joles JA, Grone HJ, Martasek P, van Zonneveld AJ, Vanin AF, Rabelink TJ: Anti-inflammatory effects of tetrahydrobiopterin on early rejection in renal allografts: Modulation of inducible nitric oxide synthase. Faseb J 2002;16:1135-1137.
34 Shen GX: Oxidative stress and diabetic cardiovascular disorders: Roles of mitochondria and nadph oxidase. Can J Physiol Pharmacol 2010;88:241-248.
35 Camici GG, Schiavoni M, Francia P, Bachschmid M, Martin-Padura I, Hersberger M, Tanner FC, Pelicci P, Volpe M, Anversa P, Luscher TF, Cosentino F: Genetic deletion of p66(shc) adaptor protein prevents hyperglycemia-induced endothelial dysfunction and oxidative stress. Proc Natl Acad Sci USA 2007;104:5217-5222.
36 Pinton P, Rimessi A, Marchi S, Orsini F, Migliaccio E, Giorgio M, Contursi C, Minucci S, Mantovani F, Wieckowski MR, Del Sal G, Pelicci PG, Rizzuto R: Protein kinase c beta and prolyl isomerase 1 regulate mitochondrial effects of the life-span determinant p66shc. Science 2007;315:659-663.
37 Francia P, delli Gatti C, Bachschmid M, Martin-Padura I, Savoia C, Migliaccio E, Pelicci PG, Schiavoni M, Luscher TF, Volpe M, Cosentino F: Deletion of p66shc gene protects against age-related endothelial dysfunction. Circulation 2004;110:2889-2895.
38 Tho LL, Candlish JK, Thai AC: Correlates of diabetes markers with erythrocytic enzymes decomposing reactive oxygen species. Ann Clin Biochem 1988;25:426-431.
39 Jia J, Zhang X, Hu YS, Wu Y, Wang QZ, Li NN, Guo QC, Dong XC: Evaluation of in vivo antioxidant activities of ganoderma lucidum polysaccharides in stz-diabetic rats. Food Chem 2009;115:32-36.
40 Chen LH, Lin ZB, Li WD: Ganoderma lucidum polysaccharides reduce methotrexate-induced small intestinal damage in mice via induction of epithelial cell proliferation and migration. Acta Pharmacol Sin 2011;32:1505-1512.
41 Haendeler J, Dimmeler S: Inseparably tied: Functional and antioxidative capacity of endothelial progenitor cells. Circ Res 2006;98:157-158.
42 Wang XR, Zhang MW, Chen DD, Zhang Y, Chen AF: Amp-activated protein kinase rescues the angiogenic functions of endothelial progenitor cells via manganese superoxide dismutase induction in type 1 diabetes. Am J Physiol Endocrinol Metab 2011;300:E1135-1145.
43 Redondo-Horcajo M, Romero N, Martinez-Acedo P, Martinez-Ruiz A, Quijano C, Lourenco CF, Movilla N, Enriquez JA, Rodriguez-Pascual F, Rial E, Radi R, Vazquez J, Lamas S: Cyclosporine a-induced nitration of tyrosine 34 mnsod in endothelial cells: Role of mitochondrial superoxide. Cardiovasc Res 2010;87:356-365.
44 Moreno DM, Marti MA, De Biase PM, Estrin DA, Demicheli V, Radi R, Boechi L: Exploring the molecular basis of human manganese superoxide dismutase inactivation mediated by tyrosine 34 nitration. Arch Biochem Biophys 2011;507:304-309.